RSC Advances

ROYAL SOCIETY OF CHEMISTRY

www.rsc.org/advances

Magnetic Fe_3O_4 Carbon Aerogel and Ionic Liquid Composite Films as an Electrochemical Interface for Accelerated Electrochemistry of Glucose Oxidase and Myoglobin

Miao Li [a], Sheying Dong [a*], Nan Li [b], Hongsheng Tang [c], Jianbin Zheng [c]

[a] *College of Sciences, Xi'an University of Architecture and Technology, Xi'an, 710055, China*

[b] *Xi'an Chuanglian Huate Surface Treatment Tech. Co. Ltd., Xi'an 710055, China*

[c] *Institute of Analytical Science, Shaanxi Provincial Key Laboratory of Electroanalytical Chemistry,Northwest University, Xi'an 710069)*

*Corresponding author. Tel.: +86 29 82201203; fax: +86 29 82205332.

E-mail address: dongsyy@126.com (S.Y. Dong)

Abstract

Synthesized magnetic ferroferric oxide carbon aerogel (Fe_3O_4-CA) was characterized by Scanning electron microscope (SEM) and N_2 adsorption-desorption isotherm measurements. Subsequently, the Fe_3O_4-CA was mixed with ionic liquid (IL) to form a stable composite film, which was characterized by Atomic forcemicroscopy (AFM) and used as an electrochemical interface for accelerating electrochemistry of glucose oxidase (GOx) and myoglobin (Mb). The results demonstrated that direct electron transfer of GOx and Mb was respectively realized on the surface of Fe_3O_4-CA/IL with a pair of well-defined quasi-reversible redox peaks. The heterogeneous electron transfer rate constant (k_s) and the surface coverage (Γ*) were

calculated as 1.30 s^{-1} and 4.10×10^{-10} M cm^{-2} for Fe_3O_4-CA/IL/GOx-CPE, 0.92 s^{-1} and 2.02×10^{-9} M cm^{-2} for Fe_3O_4-CA/IL/Mb-CPE, respectively. Moreover, the immobilized Mb exhibited excellent bioelectrocartalytic activity toward the reduction of hydrogen peroxide (H_2O_2). The biosensor displayed broad linear response to H_2O_2 in the range from 10 to 1450 μM with a detection limit of 3.2 μM. The results demonstrated that Fe_3O_4-CA/IL composite films could be a potential biocompatible interface owing to their excellent electron transfer activities, abundant mesoporous structures and large specific surface area, and wide potential applications may be developed in biosensors and biocatalysis.

Keywords: Fe_3O_4-CA composite films; Ionic liquid; Direct electrochemistry; Glucose oxidase; Myoglobin.

1. Introduction

Carbon aerogel (CA), as an important three-dimension nanocarbon material, was already applied as catalyst matrix,[1] electrosorbting salt,[2,3] adsorbent,[4] chromatographic fillings, template,[5] electrode materials and hydrogen storage materials,[6,7] etc. Compared with other carbon materials, CA is one kind of hydrogels with electroconductibility, high surface area, continuous open porosity and biocompatibility.[8] In our previous work, we synthesized three kinds of different CA-based hybrid materials for immobilizing Mb to realize the detection of hydrogen peroxide (H_2O_2).[9] However, the GOx is not easily immobilized by these materials.

It is noteworthy that ferroferric oxide (Fe_3O_4) magnetic nanomaterial has numerous

great performances such as low-cost, large specific surface area and good conductivity.[10,11] What is more important, many researchers have focused on its applications of biosensing due to its superior biocompatibility and the intimate contact among the nanoparticles, biocatalyst and substrates.[12,13] For example, Yu et al[14] proposed a novel label-free immunosensor based on Ag@Fe_3O_4 and thionine-graphene sheet (TH-GS) for the sensitive detection of kanamycin, which demonstrated effective electron transfer and amplified sensitivity owing to its excellent electron transfer activities, abundant mesoporous structures and large specific surface area. In addition, nanocomposites of Fe_3O_4 and carbon materials such as graphene sheets, carbon nanotubes, multiwalled carbon nanotubes have been extensively used in electrochemistry. Ye et al[15] synthesized reduced graphene oxide/Fe_3O_4 nanocomposite (RGO/Fe_3O_4) by coprecipitation method, then a non-enzymatic hydrogen peroxide sensor was constructed based on the composite. It is expected that Fe_3O_4-CA integrated unique characters and functions of the two types of components, would be a practical material in electrochemistry with large specific surface area, adsorption, stability, biological affinity and electrochemical conductivity.

In recent years, GOx and Mb, as crucial proteins/enzymes and in human bodies possessing high catalytic activity and stability, have extensively applied in electrochemistry as ideal mode proteins/enzymes to explore redox functional properties and electron transfer reactions.[16-19] There has been great momentum materials with good biocompatibility were employed to immobilize proteins/enzymes.

For instance, by the synergistic effect between titanium dioxide (TiO_2) and carbon nanotubes, Huang et al[20] have fabricated a novel glucose biosensor based on titanium dioxide-multiwalled carbon nanotube-chitosan-nanoplatinum-glucose oxidase (TiO_2-MWNT-CS-Pt-GOx) for catalyzing glucose. Ruan et al[21] immobilized Mb onto chitosan-graphene-ionic liquid (CTS-GR-IL) composite films and the modified electrode exhibited a high electrochemical catalytic ability for reduction of trichloroacetic acid. Nevertheless, in most case, using a composite film can only achieve the direct electrochemistry of one kind of protein or enzyme. Here, we wish to address and investigate the apparent "immobilization and promotion of the electron transfer to both GOx and Mb" to construct a wide range of sensing interface by exploiting a variety of functions of composite materials. Although the diameter of GOx is not same as that of Mb molecule, it is expected that a novel composite structure of Fe_3O_4-CA will provide a conductive network for efficient charge transfer as well as more binding sites for the protein/enzyme. To the best of our knowledge, Fe_3O_4-CA was no relative application for realizing the direct electrochemistry of proteins/enzymes reported in literatures. In addition, ILs, as molten salts with the melting point close to or below room temperature, have gained increasing attention and have potential applications in electrochemical study.[22]

In our work, for the first time Fe_3O_4-CA was synthesized and dispersed by 1-butyl-3-methylimidazolium tetrafluoroborate ionic liquid ([BMIm]BF_4, IL)[23] to form Fe_3O_4-CA/IL composite films. We attempted to immobilize GOx and Mb on the composite film of carbon paste electrode, respectively. The structure and

electrochemical behaviors of GOx/Mb entrapped in Fe_3O_4-CA/IL composite film were evaluated by spectroscopy and electrochemical methods. Furthermore, an amperometric H_2O_2 biosensor was fabricated based on the direct electrochemistry of Mb.

2. Experimental section

2.1. Reagents and apparatus

Glucose oxidase (GOx) and bovine myoglobin (Mb, MW17000) were all purchased from Sigma Chemical Co., and [BMIm]BF_4 IL (99%) was purchased from Hangzhou Chemer Chemical Limited Company. Spectral purity graphite powder was obtained from China National Medicine Corporation and liquid paraffin was purchased from Tianjing Chemical Limited Company. Resorcinol (98% purity), formaldehyde (37%-40%) and H_2O_2 (30%) were obtained from Tianjing Sheng'ao Chemical Limited Company. All the chemicals were of analytical reagent grade and used without further purification. 0.1 M phosphate buffer solution (PBS) at pH 7.0 was used, while all solutions were made up with twice-distilled water.

Morphological characterization of the nanocomposite was investigated by SEM (Quanta 600FEG, USA) at an accelerating voltage of 15 kV. Samples for SEM were coated with Au films by using a vacuum spin coater. Atomic forcemicroscopy (AFM) images were obtained on a MicroNano system (ZhuoLun MicroNano Equipment Co.) operated in tapping mode. Ultraviolet-visible (UV-Vis) spectra were recorded on a Nicolet Evolution 300 spectrophotometer in 0.1 M PBS and the FT-IR spectra (KBr) were recorded on an IR-spectrometer FTIR-8400S (Shimadzu) at room temperature.

2.2. Synthesis of magnetic Fe_3O_4-CA nanocomposite

CA was firstly synthesized in ambient conditions according to a previously reported method in literature.[24, 25] The wet RF (resorcinol-formaldehyde)-gels were prepared by curing polycondensation of RF-solutions with the molar ratio of resorcinol (R, $C_6H_6O_2$): formaldehyde (F, CH_2O)=1:2, and anhydrous sodium carbonate (Na_2CO_3) used as catalyst (C) with the weight ratio of R:C=1:500. All solutions were prepared from water which had been deionized and distilled. In the traditional RF process, the above solutions was placed in a teflon tube at 50 °C for 4 days. However, microwave-assisted heat was employed in our work, which shorten the reaction time to 30 min in comparison with conventional heating. Acetone was selected as the exchange solvent for 4 times and every time was about 6 h. Next, the RF wet gels was dried at 110 °C for 5 h and CA was obtained by pyrolyzing RF aerogels in a tube reactor at 800 °C for 3 h under the N_2 protection. The reactor temperature was raised with a rate of 8-10 °C/min and then cooled down to room temperature. Secondly, 0.2 g CA powder was dispersed into distilled water, while the mixed metal precursors of $FeCl_3 \cdot 6H_2O$ and $FeSO_4 \cdot 7H_2O$ with a molar ratio of 1:2 kept for ultrasound for about 30 min. Then, the above mixed solutions were heated to 60 °C in a three-necked bottle, under nitrogen protection with vigorous stirring for 2 h. In the reaction, pH value was adjusted to 9 or 10 with ammonia water. Immediately following, the obtained solid was filtrated and washed with water and ethanol for several times to neutral. Finally, vacuum drying for 6 h at 60 °C, the magnetic Fe_3O_4-CA was prepared and its process was shown in Scheme 1.

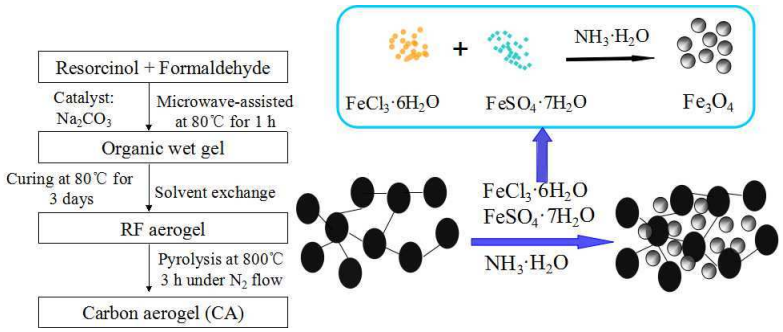

Scheme 1. Schematic diagram of the procedure to synthesize magnetic Fe_3O_4-CA

2.3. Preparation of the modified electrodes

The conduction process of carbon paste electrode (CPE) was described in **Supplementary Information.** On the basis, the GOx/Mb electrodes were prepared by a simple casting method according to the following procedures: Firstly, 2.0 mg of Fe_3O_4-CA and 10 μL $[BMIm]BF_4$ IL were dispersed into 1 mL 0.1 M PBS (pH 7.0). After sonication for 30 min, 10 μL above suspension was pipetted onto the surface of a freshly polished CPE to get Fe_3O_4-CA/IL/CPE, which was dried at room temperature. Then, 5 μL GOx (10 mg/mL) and Mb solution (5 mg/mL) was respectively casted onto the Fe_3O_4-CA/IL/CPE to obtain Fe_3O_4-CA/IL/GOx-CPE and Fe_3O_4-CA/IL/Mb-CPE, which were evaporated at 4 °C in a refrigerator to form a stable film. Finally, the modified electrodes were rinsed with doubly distilled water for twice or thrice to remove the unimmobilized protein molecules. Without use, the electrodes were stored in 0.1 M PBS (pH 7.0) at 4 °C in a refrigerator.

2.4. Electrochemical measurements

All electrochemical measurements were performed using a CHI660B workstation (Shanghai Chenhua Co., China) with a conventional three-electrode system consisting of a platinum wire auxiliary, a saturated calomel electrode (SCE) reference and a 3-mm diameter modified carbon paste electrode (CPE) working electrode. CV measurements were performed in an undivided 30 mL electrochemical teflon cell at 25 °C. Electrochemical impedance spectroscopy (EIS) measurements were carried out in 5.0 mM $K_3Fe(CN)_6/K_4Fe(CN)_6$ (1:1) mixture containing 0.1 M KCl, while the applied perturbation amplitude was 0.005 V, the frequencies swept from 10^5 to 10^{-2} Hz. For steady-state amperometric experiments, the working potential was set at -0.35 V for H_2O_2 and the solution was stirred gently with a magnetic stirrer. During electrochemical measurements, the working solutions were deoxygenated by puring with high pure nitrogen for 30 min, and nitrogen atmosphere was kept over the solution during electrochemical measurements.

3. Results and discussion

3.1. Textural properties of Fe_3O_4-CA

The morphologies of the obtained CA and Fe_3O_4-CA were examined by scanning electron microscopy (SEM) with high magnification. From the SEM image in the inset of Fig. 1A, it could be seen that the CA skeletal structure defined a nanoporous network. The continuous three-dimensional nanostructure was built by the interconnection of dozens of regular sphere-like carbon particles with diameter of about 25 nm. Similarly, the Fe_3O_4-CA image was shown in Fig. 1A consisting of

interconnected nano-sized carbon ligaments that defined a continuous polyporous network and formed lots of nano cavity or pore-like structure. Compared with CA, the slight difference was that Fe_3O_4-CA composite had more compact skeleton particles, which was ascribed to the dispersion of Fe_3O_4 particles on CA surface and insertion into the porous structure of CA. The diameter of major carbon particles that shaped irregularly ranged from 10 to 20 nm. The good connection between Fe_3O_4 particles and CA provided a porous microstructure, while induced enhancements of the adsorbing and conducting properties of the Fe_3O_4-CA host matrix, favoring for loading of proteins.

AFM images of Fe_3O_4-CA and Fe_3O_4-CA/IL composite film were investigated in Fig. 1. The surface roughnesses of the surface were assessed by vertical depth analysis of the data. The images of Fe_3O_4-CA and Fe_3O_4-CA/IL composite had numerous regular needlelike protrusions and the crater, and valley topographic features also existed, which could improve the electron transfer. Compared with Fe_3O_4-CA (Fig. 1B), the Fe_3O_4-CA/IL composite film (Fig. 1C) exhibited lower height difference, higher hierarchy. The configuration was more uniform, which could further shorten the distance and be vital in facilitating the direct electron transfer between GOx/Mb and the underlying electrode. In addition, IL not only prevented from the aggregation of Fe_3O_4-CA particles, but also performed excellent ability in acceleration of electron transfer.[26] Moreover, the FT-IR spectra of Fe_3O_4-CA/IL composite film in **Supplementary Information** indicated that the combination between Fe_3O_4-CA and IL led to an apparent increase of the intensity of the O-H

peaks, which would be benefit to the connection between GOx/Mb and composite film by numerous hydrogen bond.

Nitrogen adsorption-desorption isotherms of CA and the Fe_3O_4-CA were shown in Fig. 1D, which were both corresponded to the type IV according to IUPAC with an obvious hysteresis loop. The hysteresis effect, which is more apparent with the increase of relative pressure, appeared in the pressure of around 0.65 for CA and Fe_3O_4-CA, illustrating the presence of mesopores. There is an absorption platform when the relative pressure ranged from 0.9 to 1.0, indicating that macropore barely existed in CA and Fe_3O_4-CA. According to the textual analysis results, it can be concluded that Fe_3O_4-CA composite materials kept the carbon bone structure of CA. The plots of the pore size distribution determined by the Brunauer-Emmett-Teller (BET) method (the inset in Fig. 1D) showed that there was a dominant peak around 10 nm, and BET surface area of CA and Fe_3O_4-CA was calculated as 747 and 676 m^2 g^{-1}, respectively, much higher than other materials in Table 1. Its uniform mesopore structure and large specific surface area may be benefit to effectively immobilize of proteins/enzymes. Though CA has slightly higher surface area than Fe_3O_4-CA, the interaction between Fe_3O_4 and proteins/enzymes could improve their immobilization.

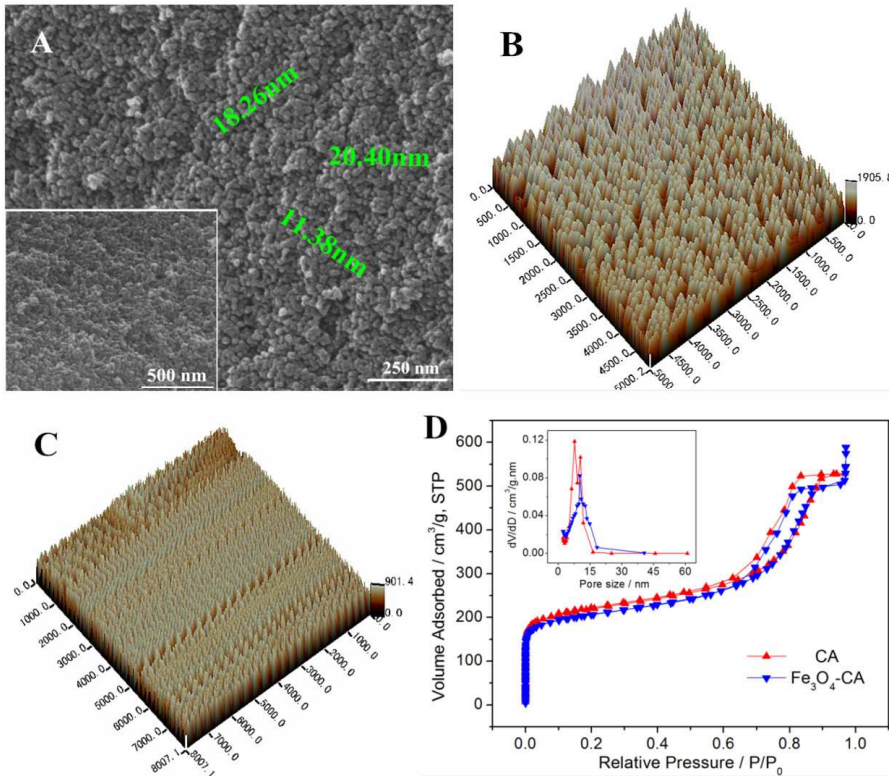

Fig. 1. (A) SEM images of Fe_3O_4-CA composite (Inset: the SEM of CA), (B) AFM image of Fe_3O_4-CA, (C) AFM image of Fe_3O_4-CA/IL composite films and (D) N_2 adsorption-desorption isotherm of CA and Fe_3O_4-CA (Inset: the pore size distribution of CA and Fe_3O_4-CA composite).

Table 1 Textual properties of different materials

Samples	BET surface area (m^2/g)	Reference
CA	747	This work
Fe_3O_4-CA	676	This work
Fe_2O_3	17.48	38
Fe_3O_4/C	8.41	38
Fe-CA	368	8

3.2. Electrochemical impedance spectroscopy

EIS was applied to monitor the whole procedure in preparing the modified electrodes, which could provide the interface information of the impedance changes between each step. In EIS, the semicircular portion at high frequencies corresponds to the electron transfer limited process and its diameter was equal to the electron transfer resistance (R_{et}), which controls the electron transfer kinetics of the redox probe at the electrode interface and the linear part at lower frequencies corresponds to the diffusion process. The R_{et} of the IL/GOx-CPE and IL/Mb-CPE was larger than that of CA/IL/GOx-CPE and CA/IL/Mb-CPE in 5.0 mM $K_3Fe(CN)_6/K_4Fe(CN)_6$ (1:1) containing 0.10 M KCl, which was ascribed to the high ionic conductivity of CA

present in the CA/IL/GOx-CPE and CA/IL/Mb-CPE. But for Fe_3O_4-CA/IL/GOx-CPE (the inset A in Fig. 2) and Fe_3O_4-CA/IL/Mb-CPE (the inset B in Fig. 2), the R_{et} were further lower compared to that of CA/IL/GOx-CPE and CA/IL/Mb-CPE, respectively. Due to electrostatic interactions, the GOx/Mb with electronegative was easily loaded on the surface of Fe_3O_4 particles with electropositive. It meant that Fe_3O_4-CA provided a more suitable orientation for GOx/Mb than CA, reducing the hindrance of protein/enzyme to electron transfer.

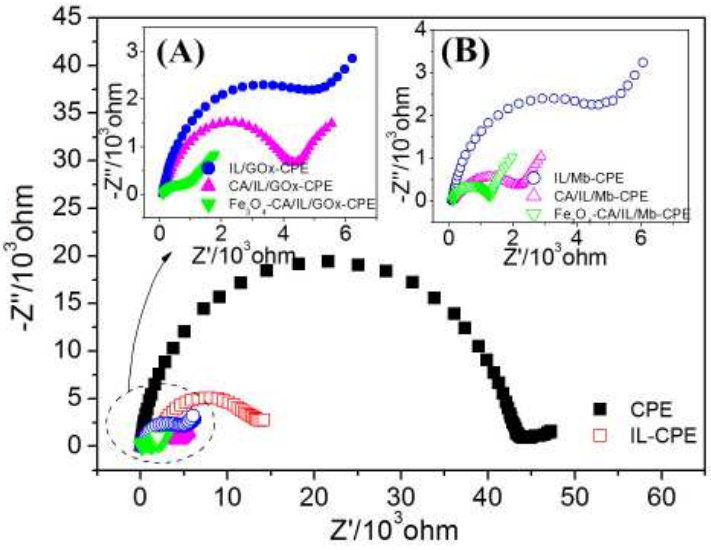

Fig. 2. Electrochemical impedance spectra (EIS) of CPE, IL-CPE, (inset A) IL/GOx-CPE, CA/IL/GOx-CPE, Fe_3O_4-CA/IL/GOx-CPE and (inset B) IL/Mb-CPE, CA/IL/Mb-CPE, Fe_3O_4-CA/IL/Mb-CPE. Supporting solution: 5.0 mM $K_3Fe(CN)_6/K_4Fe(CN)_6$ (1:1) containing 0.10 M KCl.

3.3. Direct Electrochemistry of the modified electrodes

The direct electron transfer of GOx and Mb in different modified electrodes was studied by cyclic voltammetry in 0.1 M pH 7.0 PBS respectively. As expected, no obvious electrochemical responses occurred at GOx-CPE (curve a in Fig. 3A) and Mb-CPE (curve a in Fig. 3B), which indicated that the direct electrochemistry of GOx and Mb was not achieved on bare CPE. At IL/GOx-CPE (curve b in Fig. 3A) and IL/Mb-CPE (curve b in Fig. 3B), a couple of unstable redox peaks was observed, revealing a slow electron transfer process because of the molecular film formed by water-miscible ionic liquid with the abilities of high ionic conductivity and facilitating direct electron transfer.[27] For CA/IL/GOx-CPE (curve c in Fig. 3A) and CA/IL/Mb-CPE (curve c in Fig. 3B), the redox peaks were weak. Moreover, at the Fe_3O_4-CA/IL/GOx-CPE (curve d in Fig. 3A), a pair of well-defined and quasi-reversible redox peaks was observed with the anodic peak potential ($E_{p,a}$) at -0.445 V and the cathodic peak potential ($E_{p,c}$) at -0.501 V with the formal potential $E^{0'}$=-0.473 V. Similarly, for Fe_3O_4-CA/IL/Mb-CPE (curve d in Fig. 3B), the responses of Mb were significantly enhanced and their reversibility improved greatly with anodic and cathodic peak potentials ($E_{p,a}$=-0.254 V, $E_{p,c}$=-0.404 V) as well as the formal potential $E^{0'}$=-0.329V. The phenomena were the characteristic of GOx $FAD/FADH_2$ and Mb heme Fe(III)/Fe(II) redox couple respectively.

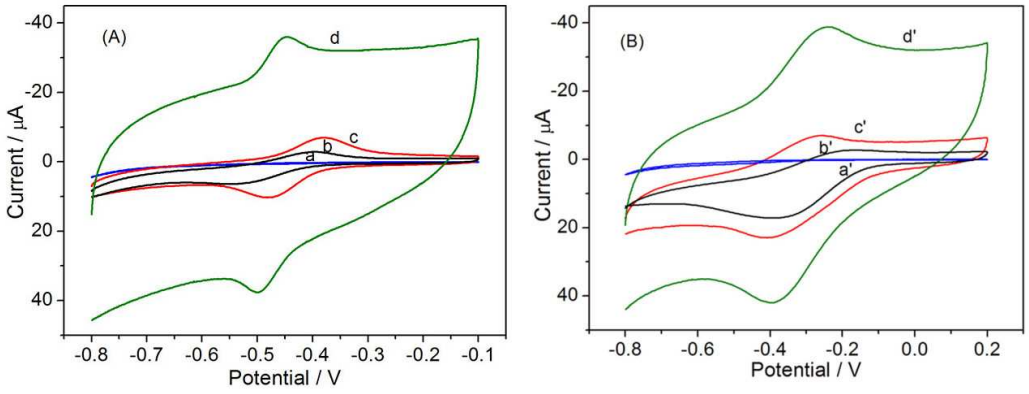

Fig. 3. (A) Cyclic voltammograms of (a) GOx-CPE, (b) IL/GOx-CPE, (c) CA/IL/GOx-CPE, (d) Fe_3O_4-CA/IL/GOx-CPE. (B) Cyclic voltammograms of (a') Mb-CPE, (b') IL/Mb-CPE, (c') CA/IL/Mb-CPE, (d') Fe_3O_4-CA/IL/Mb-CPE. Supporting solution: 0.1 M pH 7.0 PBS. Scan rate: 0.1 Vs^{-1}

From the comparison of electrochemical behavior of GOx and Mb at different electrodes, it found that GOx/Mb molecules could be effectively loaded onto the surface of Fe_3O_4-CA/IL film, inducing fast direct electron transfer between proteins and the underlying electrodes. The Fe_3O_4-CA/IL microspheres covered on CPE could provide a larger surface area and multifunctional substrate for the effective immobilization of GOx/Mb.

Meantime, UV-Vis spectra and FTIR spectra of Fe_3O_4-CA/IL/GOx-CPE and Fe_3O_4-CA/IL/Mb-CPE shown in **Supplementary Information** confirmed that the GOx and Mb were both kept its native structure in the Fe_3O_4-CA/IL membrane.

3.4. The effect of scan rate

The influence of the scan rate on the electrochemical response of the modified electrode was further investigated. As shown in Fig. 4, cyclic voltammograms of Fe_3O_4-CA/IL/GOx-CPE (Fig. 4A) and Fe_3O_4-CA/IL/Mb-CPE (Fig. 4B) were recorded in the range from 0.02/0.05 to 1.0 V s^{-1}, displaying a pair of well-defined quasi-reversible redox peaks. With the increase of scan rate, the redox peak potentials were also shifted gradually. It can be seen in inset that the anodic and cathodic peak currents were both increased linearly with the scan rate (v), while the anodic peak potentials slightly shifted to the positive direction and the cathodic peak potentials to the negative direction with the increase of the scan rates. The linear regression equations can be expressed as $i_{p,a}$(μA)=–203.01v–16.851 (R=0.991) and $i_{p,c}$ (μA)= 158.92v+21.339 (R=0.991) for Fe_3O_4-CA/IL/GOx-CPE, $i_{p,a}$(μA)=–73.97v–0.43 (R=0.991) and $i_{p,c}$ (μA)=66.00v+17.70 (R=0.986) for Fe_3O_4-CA/IL/Mb-CPE, manifesting a typical surface-controlled electrochemical process. These phenomena were also observed in other protein/enzyme modified electrode.[28, 29]

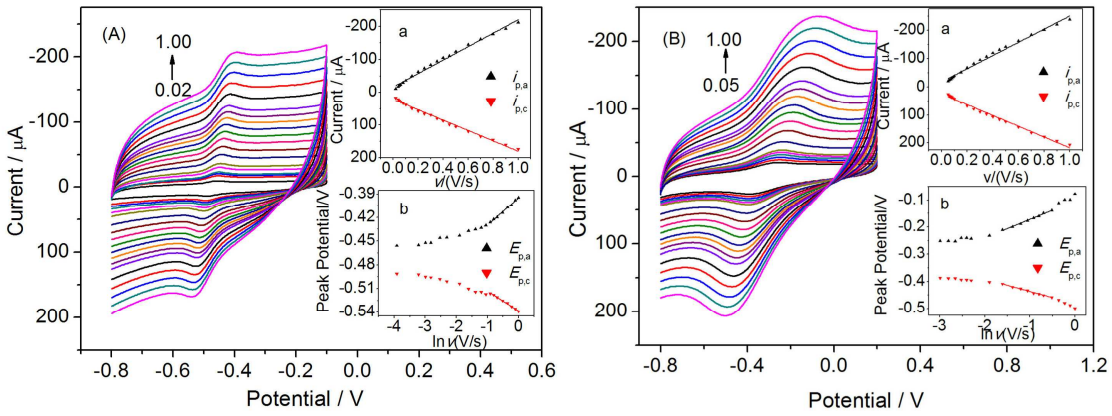

Fig. 4. Cyclic Voltammograms of (A) Fe_3O_4-CA/IL/GOx-CPE, (B) Fe_3O_4-CA/IL/Mb-CPE in pH 7.0 PBS with scan rates from 0.02/0.05 to 1.00V s^{-1}.

(The scan rates were (A) 0.02, 0.04, 0.05, 0.06, 0.08, 0.10, 0.15, 0.20, 0.25, 0.30, 0.35, 0.40, 0.45, 0.50, 0.60, 0.70, 0.80, 0.90, 1.00 and (B) 0.05, 0.06, 0.07, 0.08, 0.09, 0.10, 0.15, 0.20, 0.25, 0.30, 0.35, 0.40, 0.45, 0.50, 0.60, 0.70, 0.80, 0.90, 1.00, respectively.) Insets show the plots of (a) cathodic and anodic peak currents *vs.* scan rates and (b) Relationship of peak potentials and natural logarithm of scan rates.

For a surface-controlled process, the surface coverage (Γ^*) of electroactive GOx and Mb was estimated to be 4.10×10^{-10} M cm^{-2} and 2.02×10^{-9} M cm^{-2} based on Faraday's law: $Q = nAF\Gamma^*$, which were larger than those of 2.75×10^{-11} M cm^{-2} at GOx/MWCNTs-SnS_2/Nafion/GCE,[30] 6.69×10^{-11} M cm^{-2} at GOx/CILE,[31] 1.36×10^{-10} M cm^{-2} at Mb/ZrO_2/MWCNT.[32] The value of the heterogeneous electron transfer rate constant (k_s) were calculated using Laviron's equations[33]

$$E_{p,a} = E^{0'} + RT\ln\nu/(1-\alpha)nF \quad (1)$$

$$E_{p,c} = E^{0'} - RT\ln\nu/\alpha nF \quad (2)$$

$$\log k_s = \alpha\log(1-\alpha) + (1-\alpha)\log\alpha - \log(RT/nF\nu) - (1-\alpha)\alpha nF\Delta E_p/2.3RT \quad (3)$$

Where α is the charge transfer coefficient, and the other parameters represent their usual meanings. The k_s and α values have been estimated to be 1.30 s^{-1} and 0.57 (Fe_3O_4-CA/IL/GOx-CPE), 0.92 s^{-1} and 0.52 (Fe_3O_4-CA/IL/Mb-CPE). The obtained values of k_s were larger than that of 0.135 s^{-1} GOx-MC-IL,[34] 0.59 s^{-1} Co-NPs/Mb/CILE,[35] 0.34 s^{-1} NiO-NPs/Mb/GCE,[36] and 0.65 s^{-1} CTS-Mb-GR-IL/CILE [37] in Table 2. This results proved that the large surface area of Fe_3O_4-CA facilitated the high protein/enzyme loading, accelerating electron transfer between the

immobilized GOx/Mb and the electrode, which was attributed to not only a favorable microenvironment performed by Fe_3O_4-CA but also an electron-tunneling pathway conducted by soluble cationic single-chain surfactants of IL.

Table 2 Kinetics parameters of different electrodes

Electrodes	The surface coverage (Γ*, M cm^{-2})	Heterogeneous electron transfer rate (k_s, s^{-1})	Reference
Fe_3O_4-CA/IL/GOx-CPE	4.10×10^{-10}	1.03	This work
Fe_3O_4-CA/IL/Mb-CPE	2.02×10^{-9}	0.92	This work
GOx/MWCNTs-SnS_2/Nafion	2.25×10^{-11}	-	30
GOx/CILE	6.69×10^{-11}	-	31
GOx-MC-IL	-	0.135	34
Mb/ZrO_2/MWCNT	1.36×10^{-10}	-	32
Co-NPs/Mb/CILE	-	0.59	35
NiO-NPs/Mb/GCE	-	0.34	36
CTS-Mb-GR-IL/CILE	-	0.65	37

3.5. Electrochemical performances of Fe_3O_4-CA/IL/Mb-CPE toward H_2O_2

Electrochemical performances of Fe_3O_4-CA/IL/Mb-CPE was studied using hydrogen peroxide (H_2O_2) as model compound. The amperometric responses of the Fe_3O_4-CA/IL/Mb-CPE upon successive addition of H_2O_2 to 0.1 M pH 7.0 PBS at an applied potential of -0.35 V were shown in Fig. 5. Upon addition of an aliquot of H_2O_2 to the buffer solution, the current resoponse increased and achieved 95% of the steady-state current within 7 s. The linear regression equation was got as I_p/(μA)=0.0115c(μM)+7.486 (R=0.991). The calibration curve showed linearity from 10 to 1450 μM (inset of Fig. 5), broader than the Fe_3O_4/reduced graphene oxide sheets (Fe_3O_4/RGO)[39]. The limit of detection (LOD) is calculated to be 3.2 μM (S/N=3), which is far lower than 12.0 μM for Fe_3O_4-Au magnetic nanoparticles coated horseradish peroxidase (HRP) and graphene sheets (GS)-Nafion film modified screen-printed carbon electrode (SPCE).[40]

When H_2O_2 concentration was higher than 1450 μM, a platform was observed, exhibiting a typical characteristic of Michaelis-Menten kinetics. The apparent Michaelis-Menten constant (K_m), which gives an indication of the enzyme-substrate kinetics, can be calculated from the electrochemical version of the Lineweaver-Burk plot[41]:

$$1/I_{ss} = 1/I_{max} + K_M /I_{max} \cdot 1/c \quad (5)$$

Where I_{ss} is the steady-state current after the addition of substrate, I_{max} is the maximum current measured under saturated substrate condition, and C is the bulk

concentration of the substrate. The K_m value was determined by analysis of the slope and intercept for the plot of the reciprocals of the steady-state current versus H_2O_2 concentration. The K_m value for the designed biosensor was determined to be 0.88 mM, which is implied that the present electrode exhibited a higherh affinity for H_2O_2. The value is far smaller than those of 165 mM for iron doped carbon aerogel electrodes (Fe-CA-CPEs)[8] and 108 μM for Mb/Au/polydopamine/Fe_3O_4 magnetic bionanoparticles (Mb/Au/PDA/Fe_3O_4 MBNPs),[42] thus Mb could retain higher activity in Fe_3O_4-CA/IL and the Fe_3O_4-CA/IL/Mb-CPE showed good electrocatalytic activity for the reduction of H_2O_2.

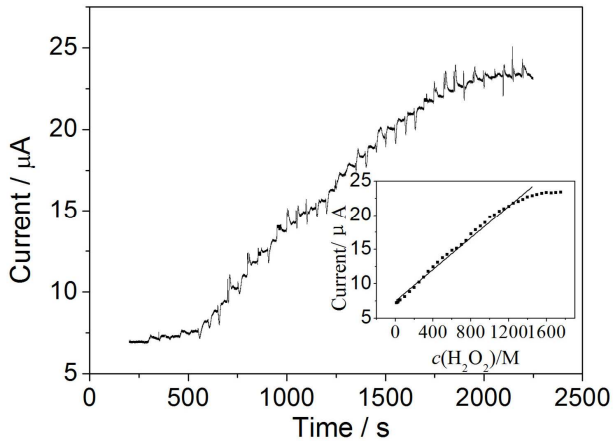

Fig. 5. Amperometric current-time response curves of Fe_3O_4-CA/IL/Mb-CPE at -0.35V (*vs*. SCE) upon successive addition of H_2O_2 into 0.1 M pH 7.0 PBS solution. Inset: calibration curve of steady-state currents *vs*. H_2O_2 concentration.

3.6. Stability and reproducibility of the GOx/Mb electrodes

Cyclic voltammetry of Fe_3O_4-CA/IL/GOx-CPE and Fe_3O_4-CA/IL/Mb-CPE in 0.1 M pH 7.0 PBS was conducted to evaluate its stability. The cyclic voltammograms changed slightly in the initial scans, and the redox peak currents almost kept nearly constant for cycles. To investigate the reproducibility between different electrodes, six electrodes were fabricated independently and relative standard deviation (RSD) of their current responses was 4.5% for Fe_3O_4-CA/IL/GOx-CPE and 3.8% for Fe_3O_4-CA/IL/Mb-CPE. After the modified electrodes were stored in a refrigerator at 4 °C, the peak current decreased to 91% and 93% of their initial responses for two weeks, respectively. The results indicated that the protein/enzyme electrodes displayed good stability and reproducibility.

4. Conclusion

The magnetic Fe_3O_4-CA and IL composite films provided more active sites for both GOx and Mb, and the direct electron transfer between the GOx/Mb and the electrode was promoted due to their abundant mesoporous structures, large specific surface area and excellent biocompatibility as well as conductivity. The sensing interface design based on the Fe_3O_4-CA/IL films was demonstrated to be effective and promising in developing protein and enzyme biosensors.

5. Acknowledgments

The authors appreciate the support from the Projects in the National Science & Technology (No. 2012BAC04B02), the Overall Innovation Project of Science & Technology in Shaanxi Province (No. 2011KTCG03-07), the Research Achievements

Foundation of Xi′an University of Architecture and Technology (No. ZC1004), and the Open Foundation of Key Laboratory of Synthetic and Natural Functional Molecule Chemistry of Ministry of Education (338080054).

References

1 M. O. Brigaudet, S. B. Fabry, C. Beauger and P. Achard, *Int. J. Hydrog. Energy.,* 2014, **39**, 1420-1429.

2 R. Chen and X. E. Hu, *Prog. Chem.,* 2006, **18**, 80-86.

3 J. Gabelich, T. D. Tran and I. H. Suffet, *Environ. Sci. Technol*., 2002, **36**, 3010-3019.

4 W. J. Yang, D. C. Wu and R. W. Fu, *J Porous Mater*., 2009, **16**, 507-512.

5 Y. M. Fang, H. Q. Hu and G. H. Chen, *Microporous. Mesoporous. Mater.*, 2008, **113**, 481-485.

6 N. P. Liu, J. Shen and D. Liu, *Electrochim. Acta*., 2013, **97**, 271-277.

7 R. G. Utke, C. Milanese, P. Javadian, J. Jepsen, D. Laipple, F. Karmi, J. Puszkiel, T. R. Jensen, A. Marini, T. Klassen and M. Dornheim, *Int. J. Hydrog. Energy*., 2013, **38**, 3275-3282.

8 C. I. Fort, L. C. Cotet, V. Danciu, G. L. Turdean and I. C. Popescu, *Mater. Chem. Phys*., 2013, **138**, 893-898.

9 S. Y. Dong, N. Li, G. C. Suo and T. L. Huang, *Anal. Chem*., 2013, **85**, 11739-11746.

10 C. Gao, X. Y. Yu, S. Q. Xiong, J. H. Liu and X. J. Huang, *Anal. Chem*., 2013, **85**, 2673-2680.

11 L. Q. Yang, X. L. Ren, F. Q. Tang and L. Zhang, *Biosens. Bioelectron*., 2009, **25**, 889-895.

12 S. M. Zhu, J. J. Guo, J. P. Dong, Z. W. Cui, T. Lu, C. L. Zhu, D. Zhang and J. Ma, *Ultrason. Sonchem*., 2013, **20**, 872-880.

13 J. H. Ji and W. Yang, *Prog. Chem*., 2010, **22**, 1566-1574.

14 S. J. Yu, Q. Wei, B. Du, D. Wu, H. Li, L. G. Yan, H. M. Ma and Y. Zhang, *Biosens. Bioelectron*., 2013, **48**, 224-229.

15 Y. P. Ye, T. Kong, X. F. Yu, Y. K. Wu, K. Zhang and X. P. Wang, *Talanta*., 2012, **89**, 417-421.

16 X. D. Shangguan, H. F. Zhang and J. B. Zheng, *Electrochem. Commun*., 2008, **10**, 1140-1143

17 H. J. Yang, T. Matsui, S. Ozaki, S. Kato, T. Ueno, G. N. Phillips, Jr., S. Fukuzumi and Y. Watanabe, *Biochem*., 2003, **42**, 10174-10181.

18 S. Ozaki, I. Hara, T. Matsui and Y. Watanabe, *Biochem*., 2001, **40**, 1044-1052.

19 S. Ray, S. Chand, Y. B. Zhang, S. Nussbaum, K. Rajeshwar and R. Perera, *Electrochim. Acta.,* 2013, **99**, 85-93.

20 X. M. Huang, X. Deng and D. Wu, *Chem. Res. Appl*., 2012, **24**, 1478-1483.

21 C. X. Ruan, T. T. Li, Q. J. Niu, M. Lu, J. Lou, W. M. Gao and W. Sun, *Electrochim. Acta*., 2012, **64**, 183-189.

22 T. Chen, H. Y. Xiong, W. Wen, X. H. Zhang and S. F. Wang, *Bioelectrochem.*, 2013, **91**, 8-14.

23 X. J. Song, B. Wang, Y. N. Huang, L. Q. Li, T. Li, C. Y. Li and S. H. Zhang, *Talanta.,* 2014, **119**, 606-612.

24 R. W. Pekala, *J. Mater. Sci*., 1989, **24**, 3221-3227.

25 S. J. KIM, S. W. HWANG and S. H. HYUN, *J. Mater. Sci*., 2005, **40**, 725-731.

26 S. Y. Dong, L. Pei, D. Liu, Q. X. Yang and T. L. Huang, *Bioelectrochem.*, 2014, **98**, 87-93.

27 K. Kwak, S. S. Kumar, K. Pyo and D. Lee, *ACS Nano*., 2014, **8**, 671-679.

28 V. Mani, B. Devadas and S. M. Chen, *Biosens. Bioelectron*., 2013, **41**, 309-315.

29 Y. Liu, Q. Y. Jiang, S. Y. Lu, Y. Zhang and H. Y. Gu, *Appl Biochem Biotechnol*., 2009, **152**, 418-427.

30 H. F. Zhang, R. X. Liu, Q. L. Sheng and J. B. Zheng, *Colloids. Surf. B: Biointerf*., 2011, **82**, 532-535.

31 X. D. Shangguan, H. F. Zhang and J. B. Zheng, *Electrochem. Commun*., 2008, **10**, 1140-1143.

32 R. P. Liang, M. Q. Deng, S. G. Cui and H. Chen, *Mater. Res. Bull*., 2010, **45**, 1855-1860.

33 E. Laviron, *J. Electroanal. Chem*., 1979, **101**, 19-28.

34 W. Sun, C. X. Guo, Z. H. Zhu and C. M. Li, *Electrochem. Commun*., 2009, **11**, 2105-2108.

35 W. Sun, X. Q. Li, P. Qin and K. Jiao, *J. Phy. Chem. C*., 2009, **113**, 11294-11300.

36 A. B. Moghaddam, M. R. Ganjali, R. Dinarvand, S. Ahadi and A. A. Saboury, *Biophys. Chem*., 2008, **134**, 25-33.

37 C. X. Ruan, T. T. Li, Q. J. Niu, M. Lu, J. Lou, W. M. Gao and W. Sun, *Electrochim. Acta*., 2012, **64**, 183-189.

38 Q. Q. Xiong, Y. Lu, X. L. Wang, C. D. Gu, Y. Q. Qiao and J. P. Tu, *J. Alloy. Compd*., 2012, **536**, 219-225.

39 S. M. Zhu, J. J. Guo, J. P. Dong, Z. W. Cui, T. Lu, C. L. Zhu, D. Zhang and J. Ma, *Ultrason. Sonochem.*, 2013, **20**, 872-880.

40 X. Yang, F. B. Xiao, H. W. Lin, F. Wu, D. Z. Chen and Z. Y. Wu, *Electrochim. Acta*., 2013, **109**, 750-755.

41 R. A. Kamin and G. S. Wilson, *Anal. Chem*., 1980, **52**, 1198-1205.

42 H. P. Peng, R. P. Liang, L. Zhang and J. D. Qiu, *J. Electroanal. Chem.*, 2013, **700**, 70-76.